Peertechz

LIFE SCIENCES GROUP

INTERNATIONAL JOURNAL OF
Nanomaterials, Nanotechnology and Nanomedicine
OPEN ACCESS JOURNAL

ISSN: 2455-3492 DOI: https://dx.doi.org/10.17352/ijnnn

Research Article

Method for Measuring Apparent Densities of Zeolite Nanopowders using Piezoelectric Energy

Jin Sun Cha[1]*, Tae Woo Kim[2], Yeon Sook Lee[1], Byeong Kon Kim[3] and Soo Kwan Jang[3]

[1]Korea testing Laboratory, Material Technology Center, 87, Digital-ro 26gil, Guro-gu 08389, Seoul, Republic of Korea

[2]Agency for Defense Development, Institute of Civil-Military Technology Cooperation, Yuseong P.O. Box 35, Daejeon, 34186, Republic of Korea

[3]Ceratorq Inc., 8, Ori-ro, 651beon-gil, Gwangmyeong, 14303, Gyeonggi-do, Republic of Korea

Received: 16 August, 2024
Accepted: 06 September, 2024
Published: 07 September, 2024

***Corresponding author:** Jin Sun Cha, Korea testing Laboratory, Material Technology Center, 87, Digital-ro 26gil, Guro-gu 08389, Seoul, Republic of Korea, Email: jscha@ktl.re.kr

ORCiD: https://orcid.org/0000-0003-3350-6051

Keywords: Zeolite; Apparent density; Piezoelectric; Flowability; Mesh plate

https://www.chemisgroup.us

Check for updates

Abstract

This study investigated factors influencing the flowability of zeolite using three types of commercial zeolites with low flowability – Zeolite-beta, Zeolite-Y, and ZSM-5 - and manufactured a device applying piezoelectric energy to measure their apparent density. Zeolite properties such as flow function (FF) and cohesion by Powder Rheometer, elemental analysis by XRF, specific surface area, pore characteristics, and shape of zeolite particles by FE-SEM, average particle size and size distribution by particle size analyzer were analyzed. Low flowability zeolite could pass through a mesh hole moved by piezoelectric energy. The apparent density measured by the device applying piezoelectric energy was found to be more uniform with a smaller standard deviation than existing density measurement equipment.

Introduction

Powder density is one of the basic properties dictating the efficiency of many processes [1]. Powder densities are typically quantified as apparent (bulk), tapped, relative, and true (absolute) densities [2]. The apparent density of a powder is the ratio of the mass of an untapped powder sample and its volume including the contribution of inter-particulate void volume [3,4]. International standard test methods for powder apparent density have been defined in various fields. Powder apparent density measurement methods standardized by International Organization for Standardization (ISO) include ISO 697 (Surface active agents – Washing powder - Determination of apparent density – Method by measuring the mass of a given volume), ISO 3923-1 (Metallic powders-Determination of apparent density-Part 1: Funnel method), ISO 9161 (Uranium dioxide powder-Determination of apparent density and tap density), ISO 23145-2 (Fine ceramics (advanced ceramics, advanced technical ceramics) - Determination of bulk density of ceramic powders – Part 2: Untapped density), and so on. These methods can measure the apparent density by calculating the mass of powder placed in a known volume container after passing through a funnel with a certain size orifice in a hoper of a certain height. To apply these methods, the powder must have flowability to pass through the orifice of the funnel. For powders that could not pass through the orifice due to low flowability, various studies have published methods to measure the apparent density using modified devices such as orifice size adjustment, vibrating funnel, modified feeding system, and so on [5-8].

Flowability is defined as the ability of a powder to flow freely regularly and constantly [9]. Flowability is affected by various properties of the powder. Ansari et al. have reported that powder flowability is not an inherent material property, but the result of a combination of many factors such as particle size, shape, particle interaction, packing fraction, flow rate, temperature, humidity, and electrostatic charge

Citation: Cha JS, Kim TW, Lee YS, Kim BK, Jang SK. Method for Measuring Apparent Densities of Zeolite Nanopowders using Piezoelectric Energy. Int J Nanomater Nanotechnol Nanomed. 2024;10(2):073-080. Available from: https://dx.doi.org/10.17352/2455-3492.000065

[10]. Stavrou et al. have also reported that powder flow is not an inherent material property but is dependent on material physical properties [11]. In the present study, a density measurement device using piezoelectric energy was developed to measure the apparent density of low-flowability powder. Piezoelectric transducers can be used to convert kinetic energy (i.e., mechanical vibration) into electrical energy (direct piezoelectric effect) or vice versa (inverse piezoelectric effect) [12-15]. These piezoelectric transducers are widely used because of their merits of simple structure, fast response, and low power consumption [16]. For example, a quartz crystal microbalance (QCM) is based on the piezoelectric effect that occurs in crystalline materials of certain crystallography [17]. QCM has been used to measure a mass variation per unit area by measuring the change in frequency of a quartz crystal resonator. QCM has been reported of exceptional importance in the fields of (bio)sensors, material science, and environmental monitoring [18]. Also, piezoelectric microbalance has been applied as a transducer for the mass of vacuum-deposited films and the mass of vapors and gases adsorbed by coatings on the crystal surface [19].

Ultrasonic vibration systems using piezoelectric transducers have been applied to various fields [20-22]. In this study, we developed a density measurement system using a piezoelectric transducer for measuring low-flowability powder. This system is similar to a conventional density measurement device except that it generates mechanical vibration to pass through a hole such as an orifice.

In this study, three types of commercial zeolites were selected as low-flowability powders. Zeolites are crystalline inorganic microporous solids formed by TO4 tetrahedra (with T=Si, Al, P, Ge, B, among others), whose structures enclose channels and/or cavities of varying size and shape [23,24]. Due to their specific pore sizes and large surface areas, zeolites have the potential for a wide range of applications such as molecular sieves, adsorbents, and catalysts [25,26]. It has been reported that the particle size of zeolite can affect reactivity [27,28]. To improve the performance of zeolite, it is necessary to apply smaller-size zeolite. However, particle size reduction can negatively impact powder flowability [29,30]. Therefore, in this study, we first studied the effects of the characteristics of three types of commercial zeolites on flowability and attempted to verify the density measurement protocol of the apparent density measurement system using piezoelectric energy.

Materials and methods

Zeolite samples

Zeolite-beta (ACS Material LLC, USA), zeolite-Y (Zeolyst, USA), and ZSM-5 (ACS Material LLC, USA) referred to as Z-B, Z-Y, and Z-5, respectively, were selected in this study. They are widely used as adsorbents and catalyst supports. Zeolite samples were heated in a convection oven for over 6 h at 110℃ and cooled in a vacuum desiccator to room temperature.

Characterization

Flowability and cohesion of zeolite were measured using a Powder Rheometer (FT4, Micromeritics). This powder rheometer can measure flow resistance while the blade moves through the zeolite powder. By measuring the rotation and vertical resistance while the blade moved through the powder, torque, and force values were obtained and then used as powder flow resistance. In this way, Flow Function (FF) and cohesion were measured. Chemical compositions of zeolites were analyzed by XRF (X-ray Fluorescence, ZSX Primus IV, Rigaku), Specific surface area and pore characteristics (pore size and volume) were analyzed using N_2 adsorption & desorption equipment after pretreatment at 150℃ for over 6 h. The shape of zeolite particles was analyzed by FE-SEM. Average particle size and size distribution were analyzed by particle size analyzer. Ethanol was used as a zeolite dispersion solvent. Before analysis, agglomerated particles were dispersed for 3 min using an ultrasonic dispersion device.

Apparent density measurement system using piezoelectric energy

Figure 1 shows a conceptual diagram of the apparent density measurement system using piezoelectric energy. It was designed to allow zeolite powder to easily pass through the sample holder by applying a piezoelectric transducer that could generate an ultrasonic vibration on a mesh plate. Figure 2(a) shows a mesh plate and Figure 2(b) shows a mesh hole designed in the form of a sieve net consisting of several mesh holes in the center. Zeolite powder on the funnel could pass through the mesh hole moved by the piezoelectric energy.

The mesh plate was designed to have an O.D. of 38 mm and an I.D. of 14 mm. The mesh hole was designed to have a square shape with an area of 0.5 mm × 0.5 mm. The mesh hole size was determined based on results obtained from a conventional apparent density measurement device. The piezoelectric transducer was manufactured by attaching piezoelectric ceramic to a mesh plate. In this study, piezoelectric ceramic with a thickness of less than 0.5 mm and an I.D. of 10 mm was used. The piezoelectric transducer was connected to an oscilloscope and set a frequency where the phase difference between the input voltage and the consumed current is 0^0 (or a frequency where the phase difference is close to 0^0).

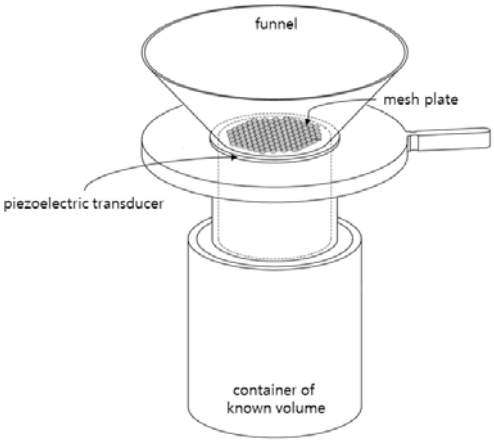

Figure 1: Schematic of an apparent density measurement device using piezoelectric energy.

Citation: Cha JS, Kim TW, Lee YS, Kim BK, Jang SK. Method for Measuring Apparent Densities of Zeolite Nanopowders using Piezoelectric Energy. Int J Nanomater Nanotechnol Nanomed. 2024;10(2):073-080. Available from: https://dx.doi.org/10.17352/2455-3492.000065

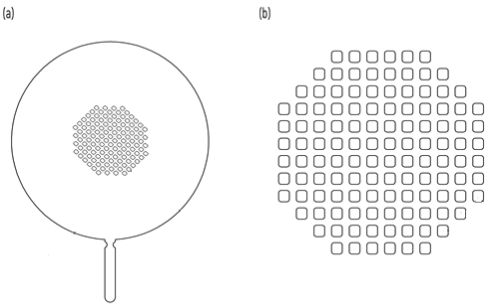

Figure 2: Diagram of mesh plate and mesh hole.

Measurement of apparent density

To measure the apparent density of zeolite powder, the mass (m_0) of a measuring container with a known empty volume was measured. The container was placed at the bottom of the funnel. According to the ISO 23145-2 standard, zeolite powder was put into a funnel with orifice sizes of 2.5, 5.0, and 10.0mm, respectively. Whether it passed through the orifice was then determined. If the zeolite powder passed through the orifice, the powder was allowed to flow into the measuring container until the container was filled with the powder and the powder overflowed its periphery. After removing the cone of surplus powder by cutting it flat with a sample knife, the mass of the measuring container containing the sample was measured (m_1). The apparent density of zeolite powder was obtained according to the following equation (1):

$$\text{Apparent density}\left(g/cm^3\right) = \frac{m_1 - m_0}{V} \quad (1)$$

Where m_0 was the mass of the empty measuring container (g), m_1 was the mass of the measuring container full of the powder (g), and V was the volume of the measuring container (cm^3).

When utilizing the apparent density measurement system using piezoelectric energy, each type of zeolite was added into the funnel shown in Figure 1. Vibration was then generated on the mesh plate to which the piezoelectric transducer was applied. Zeolite powder then passed through the mesh hole. The apparent density was determined with the same procedures as described in ISO 23145-2.

Results and discussion

Characteristics of zeolite

Table 1 shows flow function and cohesion results with a Powder Rheometer. Rheology is the study of the deformation and flow of matter [31]. Flow function measured with a Powder Rheometer represents the relationship between shear stress and normal stress of zeolite powder. The shear stress was plotted in terms of the normal stress, which is also known as τ-σ diagram [32]. The higher the shear stress for a given normal stress, the lower the flow of the powder. The shear testing protocol developed by Jenike in 1964 has been commonly used to characterize powder flow. This protocol requires measurement of consolidated stress required to shear a powder bed under a series of normal consolidation stresses [33]. Major principal stress (σ_1) and unconfined yield strength (σ_c) were identified through Mohr stress circles fitting to each yield trajectory. The ratio of the two can be expressed as a flow function (FF) as shown in equation (2)

$$\text{Flow Function}\left(\text{FF}\right) = \frac{\acute{o}_1}{\acute{o}_C} \quad (2)$$

Where σ_1 is the principal stress and σ_c is the unconfined yield strength.

Table 1 shows results at a vertical stress of 3 kPa. The higher the FF, the better the flowability. In this study, Z-B had the best flowability, followed by Z-5 and Z-Y. According to Jenike's FF classification, Z-Y and Z-5 with 2 < FF < 4 had a 'cohesive' flow behavior and Z-B with 4 < FF < 10 had an 'easy-flowing' behavior [34].

In addition, as shown in Table 1, the cohesion of Z-Y was the highest, followed by Z-5 and Z-B. This means that powders with higher cohesion have lower flowability. This result has also been reported by other researchers. Leung et al. have reported that flow function (FF) is predominantly governed by cohesion [35]. Wilkinson et al. have also reported that more cohesive powder shows poorer flowability (higher flow energy) [36].

To determine the effects of the characteristics of zeolite powder on flowability, the chemical compositions of zeolite powders were analyzed by XRF. Results are summarized in Table 2. All zeolites contained more than 90% SiO_2. Z-B and Z-Y had slightly higher SO_3 than Z-5. Z-B had higher CaO content than other zeolites but had lower contents of SO3 and CaO (below 0.5wt. %). However, the chemical compositions of zeolites were found to be similar to each other.

Table 3 shows the results of the specific surface area, pore size, and volume of zeolites. Z-Y had the highest specific surface area, followed by Z-B and Z-5. However, Z-B had the largest pore volume, followed by Z-Y and Z-5, unlike results for the specific surface area. This was because the pore size of

Table 1: Flow function and cohesion of Z-B, Z-Y, and Z-5.

	Z-B	Z-Y	Z-5
Flow function(FF)	4.28	2.43	3.89
Cohesion(kPa)	0.338	0.684	0.397

Table 2: Chemical compositions of Z-B, Z-Y, and Z-5.

(unit: wt.%)

	Z-B	Z-Y	Z-5
SiO_2	93.7	93.9	93.6
Al_2O_3	5.75	5.71	6.13
SO_3	0.241	0.242	0.061
CaO	0.110	0.006	0.017
Minor (< 0.1%)	Na_2O, MgO, P_2O_5, Cl, Fe_2O_3, CuO, Rb_2O, Y_2O_3, SnO_2, BaO	Na_2O, P_2O_5, Cl, TiO_2, Fe_2O_3, NiO, CuO, As_2O_3, SrO, ZrO_2, SnO_2, BaO	Na_2O, K_2O, TiO_2, Fe_2O_3, Br, ZrO_2, SnO_2, BaO

Citation: Cha JS, Kim TW, Lee YS, Kim BK, Jang SK. Method for Measuring Apparent Densities of Zeolite Nanopowders using Piezoelectric Energy. Int J Nanomater Nanotechnol Nanomed. 2024;10(2):073-080. Available from: https://dx.doi.org/10.17352/2455-3492.000065

Table 3: Specific surface areas and pore characteristics of Z-B, Z-Y, and Z-5.

Characteristics	Z-B	Z-Y	Z-5
BET Surface Area (m^2/g)	562.81	872.66	394.27
t-Plot Micropore Area (m^2/g)	240.40	766.61	384.98
Total pore volume (cm^3/g)	0.756	0.522	0.187
Ave. pore size (nm)	5.37	2.39	1.90

Z-B was relatively large, resulting in a large total pore volume, whereas Z-5 had micropores of less than 2 nm. Thus, the total pore volume of Z-5 was relatively low. Fitzpatrick et al. have reported that the particle surface area per unit mass is increased when particle size is decreased. When the specific surface area is increased, the surface area to interact is also increased, resulting in a more cohesive flow behavior [37]. In this study, Z-Y, which had the highest specific surface area, had the lowest flowability. However, the flowability and specific surface area didn't match for Z-B and Z-5. Abdullah et al. have also reported that the higher the specific surface area, the lower the flowability [38]. Their result was because the specific surface area increased as the particle size decreased in the same type of particulate material. However, such a result was not shown in the present study because zeolites had different pore characteristics.

Figure 3 shows the particle size distribution of zeolites. Z-B and Z-Y showed a normal distribution with mean sizes of about 450 nm and 750 nm, respectively, while Z-5 showed a double particle size distribution at 3.5 *um* and 80 *um*. Thus, the particle size of Z-5 was not uniform. Rosland Abel et al. have reported that when the particle size is reduced, the flowability is also reduced generally [34,39]. However, in the present study, Z-B having the smallest average particle size had the highest flowability. Other researchers have also reported that flowability is increased when powder has a narrower size distribution [40,41]. However, in the present study, Z-Y having the narrowest particle size distribution showed the lowest flowability, different from the results of previous studies.

FE-SEM was used to examine the particle size and shape of zeolite particles. Results are shown in Figure 4. Z-B showed a shape in which small particles less than 100 nm were agglomerated. Z-Y had an irregular shape with a larger size. Although Z-B and Z-Y had uniform particle sizes, Z-5 had particles of various sizes, similar to the results of particle size analysis. Although particle size analysis results revealed that Z-B had a wide size distribution with particle sizes of 100 nm or more, FE-SEM showed that smaller particles of Z-B were agglomerated. This indicates that Z-B cannot be dispersed into primary particles even through ultrasonic dispersion. The above results, including flow function and particle size distribution, are for agglomerated secondary particles.

Many researchers have reported that powder flowability is affected by shape factors [31,42]. We calculated the roundness and circularity of each zeolite particle based on an FE-SEM image using Image J software (version 1.54) [43]. Open the SEM image in the Image J program, and separate the color of the target particle and the background using the internal software. And then, select the range of particles to be measured using the threshold, and then calculate the size, roundness, etc. Results are shown in Figure 4 and Table 4.

When measuring the apparent density of zeolite, the size of the orifice (or mesh hole) that the zeolite particle must pass through was 2.5 to 10.0 mm. When passing through the orifice (or mesh hole) of this size, zeolite particles are expected to pass in a state of agglomerated secondary particles rather than in a state of primary particles. Thus, we analyzed the *Roundness* and *Circularity* of secondary particles using ImageJ software. Results shown in Table 4 are average values of *Roundness* and *Circularity* results from three FE-SEM images. The *Roundness* of zeolite secondary particles was calculated with equation (3) [44,45]:

$$\text{Roundness} = \frac{4A}{\delta \times R^2} \quad (3)$$

Where A was the area of the zeolite particle and R was the large axis of the zeolite particle.

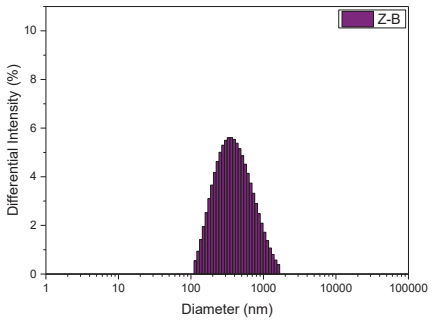

(a) Z-B

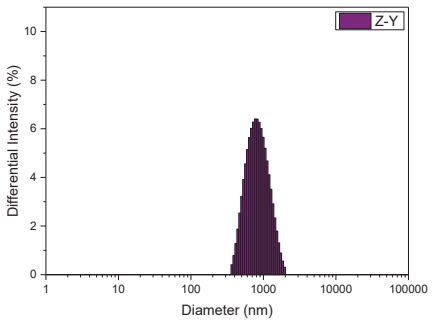

(b) Z-Y

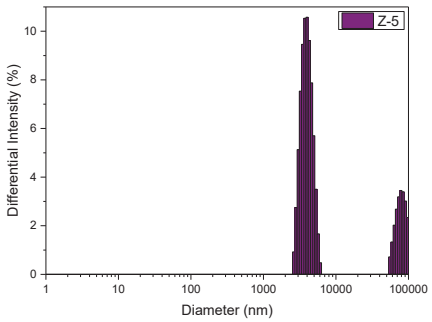

(c) Z-5

Figure 3: Particle size distribution of Z-B, Z-Y, and Z-5.

Citation: Cha JS, Kim TW, Lee YS, Kim BK, Jang SK. Method for Measuring Apparent Densities of Zeolite Nanopowders using Piezoelectric Energy. Int J Nanomater Nanotechnol Nanomed. 2024;10(2):073-080. Available from: https://dx.doi.org/10.17352/2455-3492.000065

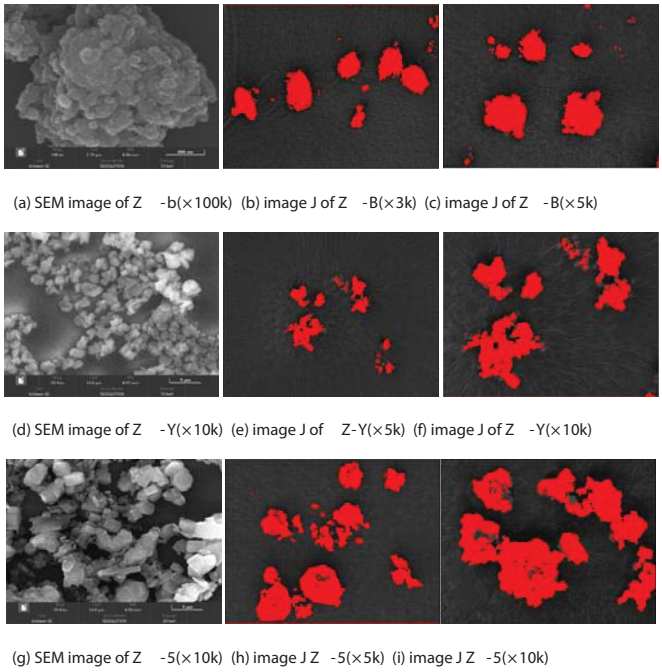

(a) SEM image of Z -b(×100k) (b) image J of Z -B(×3k) (c) image J of Z -B(×5k)

(d) SEM image of Z -Y(×10k) (e) image J of Z-Y(×5k) (f) image J of Z -Y(×10k)

(g) SEM image of Z -5(×10k) (h) image J Z -5(×5k) (i) image J Z -5(×10k)

Figure 4: SEM images and ImageJ analysis of Z-B, Z-Y, and Z-5.

Z-B had the highest *Roundness* of about 0.67, followed by Z-5 and Z-Y. Kim et al. have reported that cohesiveness is stronger for powders with low roundness and explained that this is due to friction between oval-shaped particles or particles with satellite powders [34].

Particle *Circularity* is the degree to which particles resemble a circle. It was calculated with equation (4) [46]:

$$\text{Circularity} = \sqrt{\frac{4\pi A}{P^2}} \quad (4)$$

Where A was the area of the zeolite particle and P was the perimeter length of the zeolite particle.

Z-B also had the highest *Circularity* of 0.76, followed by Z-5 and Z-Y, similar to the results of Roundness. Liu et al. have performed theoretical analysis and reported that irregularly shaped particles have poor flowability [41]. This study also found that the lower the *Roundness* and *Circularity*, the lower the flowability.

Additionally, the irregularity of each zeolite was analyzed using ImageJ software. *Irregularity* evaluates the irregularity of particle shape based on the relationship between the diameter of the maximum inscribed circle (d_{imax}) and that of the minimum circumscribed circle (d_{cmin}). It was calculated with the following equation:

$$\text{Irregularity} = \frac{d_{imax}}{d_{cmin}} \quad (5)$$

Where d_{imax} was the diameter of the maximum inscribed circle and d_{cmin} was the diameter of the minimum circumscribed circle.

When irregularity is close to 1, the particle is closer to having a sphere shape. As shown in Table 4, the *Irregularity* of Z-B was 1.50, which was the closest to 1, followed by Z-5 and Z-Y. These results were similar to the results of *Roundness* and *Circularity*. Various researchers have reported that spherical agglomeration or crystallization can improve the flowability [47-49]. It was believed that agglomerated secondary particles of Z-B showed higher flowability than other zeolites due to their relatively high sphericity.

Apparent density measurement of zeolite

In this study, the apparent density of zeolite was first measured according to the ISO 23145 Fine ceramics (advanced ceramics, advanced technical ceramics) - Determination of bulk density of ceramic powders – Part 2: Untapped density. According to the standard, if the sample cannot flow through the orifice funnel with a diameter of 2.5mm, an orifice funnel with a diameter of 5.0 mm could be used. As a result of apparent density according to the standard, Z-Y and Z-5 failed to pass the orifice funnel with diameters of 2.5 and 5.0 mm. Only Z-B passed the 5.0 mm orifice funnel as shown in Table 5. As described previously, according to Jenike's FF classification, Z-B was 'Easy-flowing' while Z-Y and Z-5 were 'Cohesive'. This characteristic was revealed when the apparent density was measured.

When apparent density was measured with a density measuring device that applied piezoelectric energy, simulation was first performed for acceleration changes according to mesh plate voltage. Figure 5 shows acceleration results for each piezoelectric transducer position at the resonant frequency. Change in acceleration according to voltage was expressed numerically, targeting the center with the highest acceleration.

In this simulation, equations (6) ~ (8) were applied to calculate acceleration [50]. Displacement of the piezoelectric transducer can be expressed with equation (6). When differentiated with time, it can be expressed as equation (7) for velocity and equation (8) for acceleration:

$$x(t) = A\cos(\omega t + \varphi) \quad (6)$$

Table 4: The shape factor of Z-B, Z-Y, and Z-5.

Shape of zeolite		Z-B	Z-Y	Z-5
Roundness	2nd particle	0.67	0.60	0.66
Circularity	2nd particle	0.76	0.66	0.71
Irregularity	2nd particle	1.50	1.76	1.58

Table 5: Apparent densities of Z-B, Z-Y, and Z-5 by test method.

					(g/cm³)
Test method			Z-B	Z-Y	Z-5
Traditional method	2.5 mm		not flowing	not flowing	not flowing
	5.0 mm		0.319	not flowing	not flowing
	10.0 mm	Ave.	0.333	0.183	0.194
		S.D.	0.016	0.018	0.013
Piezoelectric energy	Ave.		0.307	0.132	0.154
	S.D.		0.006	0.010	0.003

Citation: Cha JS, Kim TW, Lee YS, Kim BK, Jang SK. Method for Measuring Apparent Densities of Zeolite Nanopowders using Piezoelectric Energy. Int J Nanomater Nanotechnol Nanomed. 2024;10(2):073-080. Available from: https://dx.doi.org/10.17352/2455-3492.000065

$$v(t) = -A\omega sin(\omega t + \varphi) \quad (7)$$

$$a(t) = -A\omega^2 cos(\omega t + \varphi) \quad (8)$$

Where

x is a displacement (mm);

v is a velocity (m/s);l

a is an acceleration (m/s²); ¬

ω is an angular frequency;

t is a time(sec);

φ is an initial phase constant or phase angle;

A is an amplitude.

In equation (6), the maximum displacement is referred to as amplitude (A). When applying voltage V = 20V, the amplitude result by the simulation and the measurement using the laser displacement sensor (LK-H050, KEYENCE) are shown in Figure 6. a(t) max value was calculated to be 6.67×104 m/s2 by simulation, and 5.56×104 m/s2 by measurement, it was shown a deviation of approximately 17%.

As the voltage increased, the acceleration increased, which meant that the speed of zeolite passing through the metal plate hole was increased. As the voltage of the mesh plate increased, the measurement time was shortened, which could reduce errors such as moisture adsorption of zeolite during the measurement process. However, V_{pp} = 30 was applied and the mesh plate was heated. So the optimal voltage was selected at about 20 V_{pp}.

Table 5 summarizes the apparent density values of zeolites measured with a density-measuring device applying piezoelectric energy. To confirm the validity of these results, an orifice size of the ISO 23145 density measuring device was enlarged to 10.0 mm and results were compared. The apparent density measured by the density device using piezoelectric energy was found to be relatively lower than the density measured by ISO 23145 (orifice size = 10.0 mm). This was due to the sieving effect caused by the vibration of 0.5 mm mesh holes, where agglomerated zeolite powder was partially dispersed and filled into the measuring container. However,

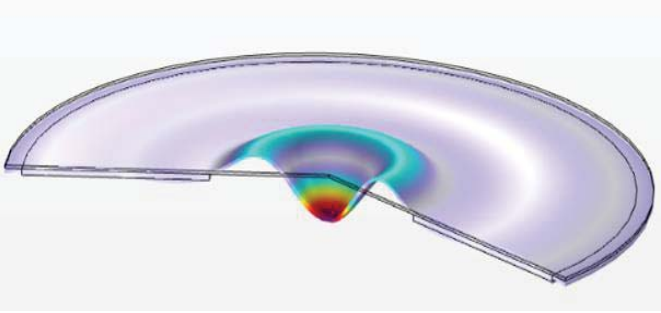

Figure 5: Simulation of transducer motion at resonant frequency.

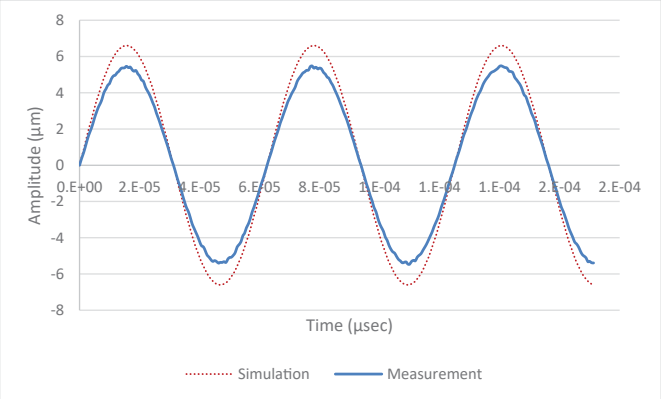

Figure 6: Amplitude measurement results by simulation and measurement.

all agglomerated zeolite powder passed through the 10.0 mm orifice of the ISO 23145 device and filled into the measuring container. The standard deviation (SD) for three measurements was also calculated to be low with the density device using piezoelectric energy, showing more uniform results.

Conclusion

In this study, we examined factors influencing the flowability of zeolite for three types of commercial zeolite with low flowability, designed an apparent density measurement device using piezoelectric energy, and verified the apparent density measurement protocol of this device. The flowability of zeolite was found to be more affected by the shape of secondary particles, such as roundness, circularity, and irregularity, rather than by characteristics such as specific surface area, particle size, or distribution. In addition, on the apparent density measurement system using piezoelectric energy, the agglomerated zeolite powder was relatively dispersed due to a sieving effect of the mesh plate. As a result, the apparent density measurement system using piezoelectric energy showed lower density values than existing density measurement equipment. It also showed more uniform results with a smaller standard deviation (S.D).

Acknowledgment

This work was supported by the Industrial Strategic Technology Development Program-Nano product performance and safety evaluation technology development and corporate support project(20015633)-funded by the Ministry of Trade, Industry & Energy (MOTIE), Republic of Korea.

References

1. Kalman H, Portnikov D. Analyzing bulk density and void fraction: B. Effect of moisture pressure. Powder Technol. 2021;381:285–297. Available from: https://doi.org/10.1016/j.powtec.2020.12.019

2. Stranzinger S, Markl D, Khinast JG, Paudel A. Review of sensing technologies for measuring powder density variations during pharmaceutical solid dosage form manufacturing. Trends Anal Chem. 2021;135:116147. Available from: https://doi.org/10.1016/j.trac.2020.116147

3. Raj K. Effect of WO3 powder particle shape, size and bulk density, on the grain size and grain size distribution of tungsten metal powder. Met Powder Rep. 2016;71:285-287. Available from: https://doi.org/10.1016/j.mprp.2016.05.007

Citation: Cha JS, Kim TW, Lee YS, Kim BK, Jang SK. Method for Measuring Apparent Densities of Zeolite Nanopowders using Piezoelectric Energy. Int J Nanomater Nanotechnol Nanomed. 2024;10(2):073-080. Available from: https://dx.doi.org/10.17352/2455-3492.000065

4. Buczek B. Measurement of the apparent density of porous particles by a powder characteristics tester. Adv Powder Technol. 1991;2:315-319. Available from: https://doi.org/10.1016/S0921-8831(08)60698-6

5. Ishii K, Suzuki M, Segawa T, Kihara Y, Yasuda M, Matsusaka S. A vibrating tube method for evaluating flowability of a small amount. Adv Powder Technol. 2011;22:522–525. Available from: https://doi.org/10.1016/j.apt.2010.07.008

6. Jiang Y, Matsusak S, Masuda H, Qian Y. Development of measurement system for powder flowability based on vibrating capillary method. Powder Technol. 2009;188:242–247. Available from: https://doi.org/10.1016/j.powtec.2008.05.003

7. Santomaso A, Lazzaro P, Canu P. Powder flowability and density ratios: the impact of granules packing. Chem Eng Sci. 2003;58:2857–2874. Available from: https://doi.org/10.1016/S0009-2509(03)00137-4

8. Hunt ML, Weathers RC, Lee AT, Brennen CE, Wassgren CR. Effects of horizontal vibration on hopper flows of granular materials. Phys Fluids. 1999;11:68-75. Available from: https://doi.org/10.1063/1.869903

9. Traina K, Cloots R, Bontempi S, Lumay G, Vandewalle N, Boschini F. Flow abilities of powders and granular materials evidenced from dynamical tap density measurement. Powder Technol. 2013;235:842–857. Available from: https://doi.org/10.1016/j.powtec.2012.11.039

10. Ansari MS, Annabattula RK, Subbiah S. Gravity-driven powder flow and the influence of external vibration on flow characteristics. Particuology. 2024;88:201-209. Available from: https://doi.org/10.1016/j.partic.2023.08.023

11. Stavrou AG, Hare C, Hassanpour A, Wu C-Y. Investigation of powder flowability at low stresses: Influence of particle size and size distribution. Powder Technol. 2020;364:98-114. Available from: https://doi.org/10.1016/j.powtec.2020.01.068

12. Tateyama A, Orino Y, Ito Y, Shiraishi T, Shimizu T, Kurosawa MK, et al. Simultaneous high-frequency measurement of direct and inverse transverse piezoelectric coefficients of thin films using longitudinal vibration. Sens Actuators A Phys. 2023;354:114265. Available from: https://doi.org/10.1016/j.sna.2023.114265

13. Mishra AK, Janani Kavi Priya VS, Pradeep K, Sai Vaishnav J, Kabhilesh G. Smart materials for ultrasonic piezoelectric composite transducer: A short review. Mater Today Proc. 2022;62:2064-2069. Available from: https://doi.org/10.1016/j.matpr.2022.02.514

14. Raihan Mohammad Siddique A, Mahmud S, Van Heyst B. A comprehensive review on vibration based micro power generators using electromagnetic and piezoelectric transducer mechanisms. Energy Convers Manag. 2015;106:728-747. Available from: https://doi.org/10.1016/j.enconman.2015.09.071

15. Batra K, Sinha N, Kumar B. Effect of Nd-doping on 0.95(K0.6Na0.4) NbO3-0.05(Bi0.5Na0.5)ZrO3 ceramics: Enhanced electrical properties and piezoelectric energy harvesting capability. J Phys Chem Solids. 2022;170:110953. Available from: https://doi.org/10.1016/j.jpcs.2022.110953

16. Du Y, Du W, Lin D, Ai M, Li S, Zhang L. Recent progress on hydrogel-based piezoelectric devices for biomedical applications. Micromachines. 2023;14:167. Available from: https://doi.org/10.3390/mi14010167

17. Ward MD, Buttry DA. In situ interfacial mass detection with piezoelectric transducers. Science. 1990;249(4972):1000–1007. Available from: https://doi.org/10.1126/science.249.4972.1000

18. Vashist SK, Vashist P. Recent advances in quartz crystal microbalance-based sensors. J Sens. 2011;2011:1–13. Available from: https://doi.org/10.1155/2011/571405

19. Olin JG, Sem GJ. Piezoelectric microbalance for monitoring the mass concentration of suspended particles. Atmos Environ (1967). 1971;5(8):653–668. Available from: https://doi.org/10.1016/0004-6981(71)90123-5

20. Hemsel T, Twiefel J. Piezoelectric ultrasonic power transducers. In: Encyclopedia of Materials: Electronics. 1st ed. 2023;276-285. Available from: https://doi.org/10.1016/B978-0-12-819728-8.00047-4

21. Zhang X, Liang B. Piezoelectric ultrasonic transducer for longitudinal-flexural vibrational mode-conversion. Appl Acoust. 2018;129:284–290. Available from: https://doi.org/10.1016/j.apacoust.2017.08.009

22. Zhang Q, Shi S, Chen W. An electromechanical coupling model of a longitudinal vibration type piezoelectric ultrasonic transducer. Ceram Int. 2015;41–S644. Available from: https://doi.org/10.1016/j.ceramint.2015.03.200

23. Muraoka K, Chaikittisilp W, Okubo T. Energy analysis of aluminosilicate zeolites with comprehensive ranges of framework topologies, chemical compositions, and aluminum distributions. J Am Chem Soc. 2016;138:6184-6193. Available from: https://doi.org/10.1021/jacs.6b01341

24. Newsam JM. The Zeolite Cate structure. Science. 1986;231:1093-1099. Available from: https://doi.org/10.1126/science.231.4742.1093

25. Wang S, Peng Y. Natural zeolites as effective adsorbents in water and wastewater treatment. Chem Eng J. 2010;156:11-24. Available from: https://doi.org/10.1016/j.cej.2009.10.029

26. Du X, Wu E. Porosity of microporous zeolite A, X, and ZSM-5 studied by small angle X-ray scattering and nitrogen adsorption. J Phys Chem Solids. 2007;68:1692-1699. Available from: https://doi.org/10.1016/j.jpcs.2007.04.013

27. Wen D, Ho Y-S, Tang X. Comparative sorption kinetic studies of ammonium onto zeolite. J Hazard Mater. 2006;133:252-256. Available from: https://doi.org/10.1016/j.jhazmat.2005.10.020

28. Lemić J, Kovačević D, Tomašević-Čanović M, Kovačević D, Stanić T, Pfend R. Removal of atrazine, lindane, and diazinone from water by organo-zeolites. Water Res. 2006;40:1079–1085. Available from: https://doi.org/10.1016/j.watres.2006.01.001

29. Ajabshir SZ, Gucuyener C, Vivacqua V, Gobby D, Stitt H, Barletta D, et al. Flow behaviour of zeolite powders at high process temperatures. Powder Technol. 2022;409:117818. Available from: https://doi.org/10.1016/j.powtec.2022.117818

30. Stavrou AG, Hare C, Hassanpour A, Wu C-Y. Investigation of powder flowability at low stresses: Influence of particle size and size distribution. Powder Technol. 2020;364:98–114. Available from: https://doi.org/10.1016/j.powtec.2020.01.068

31. Youssry M, Lemaire E, Caillard B, Colin A, Dufour I. On-chip characterization of the viscoelasticity of complex fluids using microcantilevers. Meas Sci Technol. 2012;23(12):125306. Available from: https://iopscience.iop.org/article/10.1088/0957-0233/23/12/125306

32. Wang Y, Koynov S, Glasser BJ, Muzzio FJ. A method to analyze shear cell data of powders measured under different initial consolidation stresses. Powder Technol. 2016;294:105–112. Available from: https://doi.org/10.1016/j.powtec.2016.02.027

33. Saw HY, Davies CE, Jones JR, Paterson AHJ. Shear testing of lactose powders: The influence of consolidation stress and particle size on bulk density and estimated cohesion. Adv Powder Technol. 2014;25:1164-1170. Available from: https://doi.org/10.1016/j.apt.2014.05.009

34. Kim TY, Kang MH, Kim JH, Hong JK, Yu JH, Lee JI. Effect of particle sphericity on the rheological properties of Ti-6Al-4V powders for laser powder bed fusion process. J Powder Mater. 2012;29:99-109. Available from: https://doi.org/10.4150/KPMI.2022.29.2.99

Citation: Cha JS, Kim TW, Lee YS, Kim BK, Jang SK. Method for Measuring Apparent Densities of Zeolite Nanopowders using Piezoelectric Energy. Int J Nanomater Nanotechnol Nanomed. 2024;10(2):073-080. Available from: https://dx.doi.org/10.17352/2455-3492.000065

35. Leung LY, Mao C, Srivastava I, Du P, Yang C-Y. Flow function of pharmaceutical powders is predominantly governed by cohesion, not by friction coefficients. J Pharm Sci. 2017;106:1865–1873. Available from: https://doi.org/10.1016/j.xphs.2017.04.012

36. Wilkinson SK, Turnbull SA, Yan Z, Stitt EH, Marigo M. A parametric evaluation of powder flowability using a Freeman rheometer through statistical and sensitivity analysis: A discrete element method (DEM) study. Comput Chem Eng. 2017;97:161–174. Available from: https://doi.org/10.1016/j.compchemeng.2016.11.034

37. Fitzpatrick JJ, Barringer SA, Iqbal T. Flow property measurement of food powders and sensitivity of Jenike's hopper design methodology to the measured values. J Food Eng. 2004;61:399–405. Available from: https://doi.org/10.1016/S0260-8774(03)00147-X

38. Abdullah EC, Salam AM, Aziz AR. Cohesiveness and flowability properties of silica gel powder. Phys Intl. 2010;1:16–21. Available from: https://doi.org/10.3844/pisp.2010.16.21

39. Rosland Abel SE, Yusof YA, Chin NL, Chang LS, Ghazali HM, Ghani MA, et al. The effect of particle size on the physical properties of Arabic gum powder. J Food Process Eng. 2020;43:1-12. Available from: https://doi.org/10.1111/jfpe.13368

40. Lumay G, Boschini F, Traina K, Bontempi S, Remy J-C, Cloots R, et al. Measuring the flowing properties of powders and grains. Powder Technol. 2012;224:19–27. Available from: https://doi.org/10.1016/j.powtec.2012.02.015

41. Liu LX, Marziano I, Bentham AC, Litster JD, White ET, Howes T. Effect of particle properties on the flowability of ibuprofen powders. Int J Pharm. 2008;362:109–117. Available from: https://doi.org/10.1016/j.ijpharm.2008.06.023

42. Fu X, Huck D, Makein L, Armstrong B, Willen U, Freeman T. Effect of particle shape and size on flow properties of lactose powders. Particuology. 2012;10:203–208. Available from: https://doi.org/10.1016/j.partic.2011.11.003

43. Schneider CA, Rasband WS, Eliceiri KW. NIH Image to ImageJ: 25 years of image analysis. Nat Methods. 2012;9:671–675. Available from: https://doi.org/10.1038/nmeth.2089

44. Flórez-Acosta O, Tobón-Zapata G, Valencia-Velasquez J. Categorization of the main descriptors of different ampicillin crystal habits. Braz J Pharm Sci. 2010;46:679–685. Available from: https://doi.org/10.1590/S1984-82502010000400009

45. Atwater MA, Luckenbaugh TL, Hornbuckle BC, Darling KA. Solid state foaming of nickel, Monel, and copper by the reduction and expansion of NiO and CuO dispersions. Adv Eng Mater. 2018;46:1800302. Available from: https://doi.org/10.1002/adem.201800302

46. Cox EP. A method of assigning numerical and percentage values to the degree of roundness of sand grains. J Paleontol. 1927;1:179–183. Available from: https://www.jstor.org/stable/1298056

47. Chen H, Wang C, Sun CC. Profoundly improved plasticity and tabletability of griseofulvin by in-situ solvation and desolvation during spherical crystallization. Cryst Growth Des. 2019;19:2350–2357. Available from: https://doi.org/10.1021/acs.cgd.9b00053

48. Nokhodchi A, Maghsoodi M, Hassan-Zadeh D, Barzegar-Jalali M. Preparation of agglomerated crystals for improving flowability and compactibility of poorly flowable and compactible drugs and excipients. Powder Technol. 2007;175:73–81. Available from: https://doi.org/10.1016/j.powtec.2007.01.030

49. Kawashima Y, Imai M, Takeuchi H, Yamamoto H, Kamiya K, Hino T. Improved flowability and compactibility of spherically agglomerated crystals of ascorbic acid for direct tableting designed by spherical crystallization process. Powder Technol. 2003;130:283–289. Available from: https://doi.org/10.1016/S0032-5910(02)00206-1

50. Ozerov RP, Vorobyev AA. Oscillations and Waves, Physics for Chemists. 2007;105-167. Available from: https://doi.org/10.1016/b978-044452830-8/50004-0

Citation: Cha JS, Kim TW, Lee YS, Kim BK, Jang SK. Method for Measuring Apparent Densities of Zeolite Nanopowders using Piezoelectric Energy. Int J Nanomater Nanotechnol Nanomed. 2024;10(2):073-080. Available from: https://dx.doi.org/10.17352/2455-3492.000065